Environmental Science Nano

ROYAL SOCIETY OF CHEMISTRY

PAPER

View Article Online
View Journal | View Issue

Cite this: *Environ. Sci.: Nano*, 2025, 12, 2857

The surface charge both influences the penetration and safety of polystyrene nanoparticles despite the protein corona formation†

Giulia Yuri Moscatiello,[a] Carmina Natale,[a] Mariagiovanna Inserra,[a] Annalisa Morelli,[a] Luca Russo,[a] Nora Battajini,[a] Laura Sironi,[b] Davide Panzeri,[b] Alessandro Corbelli,[a] Ada De Luigi,[a] Fabio Fiordaliso,[a] Gabriele Candiani,[c] Paolo Bigini*[a] and Luisa Diomede*[a]

Received 14th October 2024,
Accepted 31st March 2025

DOI: 10.1039/d4en00962b

rsc.li/es-nano

Micro- and nano-plastics' (MNPs') environmental persistence generates relevant alarm. This concern is amplified for non-biodegradable materials like polystyrene (PS). It is known that MNPs easily penetrate cells and accumulate in vital organs. Despite the great interest, a univocal idea about MNPs' toxicity is still lacking. In this study, PS-nanoparticles (PS-NPs) were employed as prototypic material. We focused our attention on the role played by the external surface in the internalization and toxicity of amine- and carboxylate-modified fluorescent PS-NPs with different z-potentials. Human embryonic kidney (HEK) 293 cells and *C. elegans* have been employed to model the effects of PS-NPs *in vitro* and *in vivo*. Both positive and negative PS-NPs entered cells primarily by clathrin-mediated endocytosis and were rapidly trapped by lysosomes. However, amine-modified positive NPs were more uptaken than negative ones and caused a dose-dependent decrease in cell growth and viability in HEK 293 cells. Internalized NPs and their mean distance from the cell nucleus have also been quantitatively characterized through a dedicated Cell Profiler-Matlab pipeline. The z-potential of PS-NPs also affected their toxic effect *in vivo*, being only positive NPs able to cause a dose-related decrease of *C. elegans* viability and defects in motility, pharyngeal function, reproduction, and development. These results underline the crucial role of the surface charge of PS-NPs in their interaction with cell membranes and *in vitro* and *in vivo* biological effects.

Environmental significance

Since the last century, the extensive development of polymer chemistry has led to a revolution in industry production and market consumption. Plastics are now almost everywhere, and due to their limited lifespan and insufficient recycling, there is an overload in the environment, where they can potentially interact with animals and humans. Although the effect of macro-plastics has been extensively investigated, the interaction between nanoplastics and biological targets is far from being clarified. Understanding how factors, such as the external surface charge, impact the protein corona formation and influence the environment and health is needed to improve sustainable plastics production. Although the present study does not provide definitive indications for regulatory risk assessment, it confirms that any single physico-chemical feature characterizing nanoplastic cannot be neglected.

1. Introduction

Plastic production can be considered one of the main revolutions of the last century. From the early 1950s to the last decade, the production of plastic materials has increased from 1.7 million tons per year to around 300 million tons per year.[1] The COVID-19 pandemic has further increased the demand for single-use plastic hand sanitizer bottles and face masks.[2]

[a] *Department of Molecular Biochemistry and Pharmacology, Istituto di Ricerche Farmacologiche Mario Negri IRCCS, Via Mario Negri 2, 20156 Milano, Italy. E-mail: giulia.moscatiello@marionegri.it, carmina.natale@marionegri.it, mariagiovanna.inserra@gmail.com, annalisa.morelli@marionegri.it, luca.russo@hsr.it, norachiara.battajni@mail.polimi.it, alessandro.corbelli@marionegri.it, ada.deluigi@marionegri.it, fabio.fiordaliso@marionegri.it, paolo.bigini@marionegri.it, luisa.diomede@marionegri.it*

[b] *Department of Physics, Università degli Studi di Milano-Bicocca, Milan, Italy. E-mail: laura.sironi@unimib.it, d.panzeri@campus.unimib.it*

[c] *genT_LAB, Department of Chemistry, Materials and Chemical Engineering "G. Natta", Politecnico di Milano, Milan, Italy. E-mail: gabriele.candiani@polimi.it*

† Electronic supplementary information (ESI) available. See DOI: https://doi.org/10.1039/d4en00962b

Despite campaigns for efficient waste recycling, the dispersion of plastic materials in the environment is high. Its erosion and consequent disaggregation often follow plastic release in micro- and nano-plastics (MNPs).

MNPs are universally recognized as one of the most relevant pollution-related issues to understand. In addition to their direct effects, MNPs can interact with a broad range of matrices representing an "eco-toxicology" issue impacting animal and human health.[1] In particular, through the food chain, MNPs may accumulate in animals and human bodies and deposit in various organs, exerting a toxic effect.[3,4] MNPs' ability to enter the cells has been widely investigated, and their effect depends not only on the type of polymers used. Still, it can dramatically change if the same type of plastic is used.[5,6] Indeed, although material plays a relevant role in the deformation of the cell membrane, it is widely reported that the electrical attraction between positively charged MNPs and the negative lipid bilayer strongly influences the kinetics and efficiency of their uptake.[7,8]

The most commonly used non-biodegradable plastics are poly(vinyl chloride), polyethylene, polypropylene, poly(ethylene terephthalate), and above all, polystyrene (PS).[9] Due to its high molecular weight and low hydrophilicity, PS covers a vast spectrum of practical applications, and it is extensively utilized to produce toys, compact discs, styrofoam boxes, cup covers, and many other similar commercial products. Like other nanomaterials, PS-MNP toxicity can be strongly influenced by different physico-chemical parameters (*e.g.*, size, geometry, external charge). Therefore, robust indications about the PS-MNPs' biological effect after interacting with both environmental-biological fluids and possible contaminants, which often highly influence the z-potential and the dimensions, are crucial to forecast their potential toxicity.

The z-potential represents the overall charge of the slipping plane (*i.e.*, the cloud of ions surrounding the surface of the particles) and is affected by the surface composition of the nanoparticles (NPs). Since the overall electrical charge of the cell plasma membrane is negative, NPs characterized by a positive surface charge are easily attracted and more likely to be internalized by endocytosis.[10] Interestingly, despite increased studies using positively charged PS-NPs, few controversial data emerged from negatively charged PS-NPs.[11]

The present study was mainly devoted to characterizing the effect of z-potential in bio-nano interaction both at the single-cell level and in an invertebrate animal. To this end, human embryonic kidney (HEK) 293 cells, widely employed for nanotoxicological studies, were used as models due to the role of kidneys in the NP's excretion.[12] In addition, in a more complex scenario, the nematode *Caenorhabditis* (*C.*) *elegans* was used as an *in vivo* animal model, which has already been widely tested for nanotoxicity studies.[13] Due to the ~60% homology of its genes with humans and well-conserved molecular pathways, *C. elegans* provides a simple and low-cost model to study the toxicity of MNPs, offering relevant information on the molecular mechanisms involved. This nematode is ubiquitous worldwide, living in water and soil of arctic, subarctic, and temperate regions,[14,15] thus representing an excellent environmental indicator. *C. elegans* has also been widely employed for nanotoxicology studies, including polymeric NPs, and for correlated NP toxicity with their shape, size, and charge.[13,16–19]

To investigate the impact of surface charge in both biological models, we employed amine-modified positive and carboxylate-modified negative fluorescent PS-NPs with the same shape, size, and coating to avoid potential bias. In recent years, attention has mainly focused on the role of materials in differentiating their eco-toxicological impact on MNPs. To dig deeper into this topic, this work aims to provide details on the effects of the same material with specific chemical–physical differences. This is crucial to indicate the relevance, not only based on the degree of biodegradability of the polymeric structures.

2. Materials and methods

2.1 Nanoparticle characterization

Two different types of PS-NPs were purchased from Magsphere Inc. (Pasadena, USA): red fluorescent latex, aminated (positively charged AMFR100NM) or carboxylated (negatively charged CAFR100NM). PS-NPs were made with covalently linked rhodamine B to make them detectable by imaging techniques. For the characterization, NPs were diluted in MilliQ water at the final 2.5 μg ml^{-1} concentration. One ml of suspension was used for conducting, at room temperature, the dynamic light scattering (DLS) analysis using Delsa nano submicron particle size and zeta potential (Beckman Coulter, California, USA).

For atomic force microscopy (AFM) analysis, positive NPs were diluted in MilliQ water at the final 2.5 μg ml^{-1} concentration, and negative NPs were diluted in a 100 mM HCl solution at 2.5 μg ml^{-1}. This procedure is commonly applied to negatively charged materials to allow their adhesion to the Muscovite mica surface before the AFM analysis. However, such treatment does not modify the physico-chemical properties of negative NPs. Thirty μl of each suspension were spotted onto a freshly cleaved Muscovite mica disk, and after 5 minutes, the disk was washed with 10 ml ddH2O and dried under a gentle nitrogen stream. Samples were mounted onto a Multimode AFM with a NanoScope V system (Veeco/Digital Instruments, New York, USA) operating in tapping mode using standard antimony(n)-doped Si probes (*T*: 3.5–4.5 mm, *L*: 115–135 mm, *W*: 30–40 mm, f_0: 313–370 kHz, *k*: 20–80 N m^{-1}) (Bruker, Massachusetts, USA).

Fluorescent spectra of 0.025–50 μg ml^{-1} positive and negative PS-NPs suspended in water were registered using the spectrofluorometer Tecan Infinite 200 (Männedorf, Switzerland) at 505–545 nm excitation and 560–630 nm emission wavelengths. Fluorescence reading mode was the top reading. A black 96-well plate (Corning Incorporated Costar 3603, New York, USA) was used to avoid reading interference among adjacent wells, and 100 μl of solution

was added for each well. Water was used as blank. Each experimental condition was measured in triplicate.

2.2 Cell growth and cytotoxicity

HEK 293 cells (Merck Life Science S.r.l., Milan, Italy, cod. 85120602-1VL) were cultured in Dulbecco's modified Eagle medium (DMEM) (Gibco, Milan, Italy) supplemented with 10% heat-inactivated fetal bovine serum (FBS) (Gibco), L-glutamine (Gibco), non-essential amino acids (Gibco) penicillin/streptomycin (Corning, New York, USA), and puromycin (Genespin, Milan, Italy). Cells were maintained in T25 flasks at 37 °C in humidified 5% CO_2 and routinely split every 3–4 days.

For cell growth experiments, HEK 293 cells were seeded on 96-well plates (1×10^4 cells per well) in a complete DMEM medium with 10% FBS. Positive and negative PS-NPs in 2.5 mg ml^{-1} Milli-Q water stock solution were added to the cells at final concentrations of 2.5, 10, and 25 μg ml^{-1}. Control cells were treated with the corresponding volume of MilliQ water. Cells were incubated at 37 °C in a humidified 5% CO_2 atmosphere, and their number was determined 24, 48, and 72 hours later. To this end, the medium was removed, cells were washed with 10 mM phosphate buffered saline (PBS) and detached with trypsin–EDTA 0.25%. Cells were then counted through Vi-CELL BLU analyzer (Beckman Coulter, California, USA).

To evaluate the cytotoxic effect of NPs, HEK 293 cells were seeded on 96-well plates (2×10^4 cells per well) in a complete DMEM medium with 10% FBS. Positive and negative PS-NPs in 2.5 mg ml^{-1} Milli-Q water stock solution were added to the cells at 2.5 and 10 μg ml^{-1} concentrations. Control cells were treated with the corresponding volume of MilliQ water. After incubation for 30 minutes, 6 hours, and 24 hours at 37 °C, the viability assay was carried out with 3-(4,5-dimethylthiazol-2-yl)-2,5-diphenyltetrazolium bromide (MTT) (Sigma Aldrich, St. Louis, MO, USA). Cell viability was determined by measuring the absorbance at 560 nm using Infinite M200 (Tecan).

2.3 Imaging studies

HEK 293 cells were seeded on 8-well plates (IBIDI GmbH, Germany) (1.5×10^4 cells per 200 μl per well) for 24 hours in a complete DMEM medium with 10% FBS. Positive and negative PS-NPs in 2.5 mg ml^{-1} Milli-Q water stock solution were then added to the cells at 2.5 and 10 μg ml^{-1} concentrations. Control cells were treated with the corresponding volume of MilliQ water. Cells were incubated at 37 °C in a humidified 5% CO_2 atmosphere. Images were acquired at different time points (from 30 minutes to 24 hours) after the treatment using a confocal microscopy apparatus with a temperature, humidity, and CO_2 detector (Nikon A1 Confocal, Tokyo, Japan).

To investigate the mechanisms of NPs uptake, HEK 293 cells were seeded on 8-well plates (1.5×10^4 cells per 200 μl per well) in a complete DMEM medium with 10% FBS and incubated for 30 minutes at 37 °C in a humidified 5% CO_2 atmosphere with chlorpromazine (2.5 μg ml^{-1}) (Sigma Aldrich, Missouri, USA). Cells were then treated with 2.5 μg ml^{-1} NPs (positive and negative) for 2 hours to assess the possible inhibition of the uptake through the clathrin-mediated pathway. Images were acquired using a confocal microscope.

To identify the transport machinery vesicle-mediated that regulates positive NPs cellular uptake, HEK 293 cells were seeded in an 8-well plate (1.5×10^4 cells per 200 μl per well) and treated with 2.5 μg ml^{-1} positive PS-NPs. Twenty-four hours later the incubation at 37 °C in a humidified 5% CO_2 atmosphere, the medium was removed, the samples were fixed in 4% paraformaldehyde (PAF) solution in 10 mM PBS and immune stained using three different antibodies: the rabbit monoclonal anti-lysosomal associated membrane protein 2 (LAMP2, 1:50) (Thermofisher, New Hampshire, USA), the mouse monoclonal anti-mannose 6-phosphate receptor (M6PR, 1:100) (Abcam, Cambridge, UK) and the rabbit monoclonal anti-early endosome antigen 1 (EEA1, 1:500) (Abcam, Cambridge, UK). Two different secondary antibodies were used: a goat anti-mouse Alexa Fluor Plus 488 (A32723 Invitrogen, Massachusetts, USA) and a goat anti-rabbit Alexa Fluor Plus 647 (A32733 Invitrogen, Massachusetts, USA). Images were acquired with a confocal microscope at 40× and 100× magnification and structured illumination microscopy (Nikon N-SIM microscope).

2.4 Quantification of NPs uptake

Confocal images obtained, as described before, were converted from the ND2 Nikon file format to a multipage 3-channel TIFF with the Bioformats plugin of ImageJ. For quantification, a processing pipeline composed of a CellProfiler routine was applied to perform instance segmentation, and a MATLAB code was employed to extract the following parameters: fraction of cell area covered by NPs, mean NP intensity per cell, weighted NP intensity per cell, and NP distance from the cell nucleus. Starting from a single 3-channel image, we obtained two multi-label segmentation masks related to each cell and the relative nuclei. Each cell was segmented independently and paired with its corresponding nucleus by a shared label index. The images were loaded into CellProfiler, representing each fluorescence channel as a 16-bit grayscale image. The channel, corresponding to the DAPI nuclear marker, was segmented by global thresholding. Otsu Thresholding estimated a threshold to separate the background component from the positively stained pixels. After applying a shape-based de-clumping algorithm – included in CellProfiler - touching nuclei were split into individual objects. A similar thresholding procedure was performed on the membrane marker fluorescence channel. The previously segmented nuclei acted as seed points for a watershed algorithm that split the segmentation mask into individually labeled cell objects according to the nuclei' positions. The two multi-label segmentation masks were exported into TIFF files and were analyzed using a MATLAB script. In MATLAB, the channel representing the NP's

fluorescence emission was processed by a 3 × 3 median filter. Then, a hard-coded global threshold was employed to discard background contributions.

The fraction of cell area covered by NPs was evaluated as the number of positive pixels (above threshold) inside a cell divided by the total number of pixels belonging to a single cell.

Finally, we computed the Euclidean distances between the centroid of the cell nucleus and the centroids of all the NPs inside the cell. The distance of the internalized NPs from the cell nucleus was quantified by computing the mean distance, then normalized to the maximum Feret diameter that encloses the cell. This normalization yields a dimensionless ratio representing the NPs' mean proximity to the nucleus to the overall extent of the cell. The resulting value ranged from 0 to 1, where 0 indicates NPs closer to the nucleus and 1 near the cell membrane. The results were exported as an Excel file and later processed by GraphPad Prism v. 9.0. All cell parameters were grouped by time-point and NP charge.

After image acquisition, we exploited the ImageJ suite together with the JACoP plugin (**https://github.com/fabricecordelieres/IJ-Plugin_JACoP**) to compute the Pearson correlation coefficient between the fluorescence signals of distinct markers. The JACoP plugin supports pairwise comparison of two separate images and provides the Pearson correlation value as output.

2.5 Effect of protein corona on NPs internalization

To evaluate how the protein corona could affect the uptake of NPs into cells, PS-NPs (2.5 μg ml^{-1}) were incubated for 1 hour at 37 °C with FBS. Samples were centrifuged (1 h, 16 000 × *g*, 4 °C), and the pellet was washed three times with 10 mM PBS. The formation of the corona was evaluated by eluting the proteins from the NPs by adding SDS-sample buffer (dH_2O, 0.5 M Tris-HCl, glycerol, 10% SDS, 2-mercaptoethanol, 1% bromophenol blue) and separating the corona proteins through 10% polyacrylamide SDS/PAGE. After the electrophoresis, the gel was stained with Coomassie Blue (Sigma Aldrich, Missouri, USA) for 1 hour at room temperature with gentle shaking and destained overnight. Images were acquired at Chemidoc (Bio-Rad, Hercules, California).

To visualize the formation of the protein corona, for each group of NPs, a 10 μl drop of the suspended solution was placed at room temperature for 30 min on a 100 mesh formvar/carbon-coated copper grid (EMS, Hatfield, PA, USA). After absorbing the excess of the suspension with Whatman filter paper, the grids were observed with an Energy Filter Transmission Electron Microscope (EFTEM, ZEISS LIBRA® 120) equipped with a YAG scintillator slowscan CCD camera (Sharp eye, TRS, Moorenweis, Germany).

Positive and negative PS-NPs (2.5 μg ml^{-1}), previously incubated with serum, as previously described, were administered to HEK 293 cells. Twenty-four hours after incubation at 37 °C in a humidified 5% CO_2 atmosphere, cells were fixed with 4% PAF solution, and cell membranes and nuclei were stained respectively with WGA633 (Biotium, Fremont, California) and Hoechst 33258 (Merck, Sigma Aldrich, Darmstadt, Germany). Images were acquired with Nikon A1 Confocal Microscopy, while Virtual slide images were acquired through Olympus virtual slide microscope VS120 (Olympus, Tokyo, Japan).

2.6 *C. elegans* studies

Bristol N_2 nematodes were obtained from the *Caenorhabditis elegans* Genetic Centre (CGC, University of Minnesota, Minneapolis, MN, USA) and propagated at 20 °C on solid Nematode Growth Medium (NGM) seeded with *E. coli* OP50 (CGC) for food. Age-synchronized animals were prepared using the bleaching technique.[20] To investigate the *in vivo* toxicity of PS-NPs, *C. elegans* at the L4 larval stage were collected, centrifuged, and washed twice with 10 mM PBS, pH 7.4, to remove bacteria. Worms were then incubated for 2 hours at room temperature in orbital shaking, in the absence of *E. coli*, with increasing concentration (2.5–50 μg ml^{-1}) of PS-NPs (100 worms per 100 μl). Control worms were treated under the same experimental conditions with 10 mM PBS, pH 7.4 (100 worms per 100 μL) (vehicle). After 2 hours of orbital shaking, worms were plated onto NGM plates seeded with OP50 *E. coli* and grown at 20 °C. Survival analysis was conducted 24 hours after the NP treatment by counting the number of dead and alive worms on the plate.

To evaluate the biodistribution of NPs in worms, synchronized nematodes at the L3 larval stage were treated for 2 hours at room temperature with 10 μg mL^{-1} of positive and negative PS-NPs (100 worms per 100 μl) as described before. After 2- and 24-hour treatment, worms were mounted on a glass slide coated with 2% agarose and anesthetized with 10 mM Levamisole (Sigma). After the coverage of each slide with a coverslip, the biodistribution of PS-NPs was evaluated using an inverted fluorescence microscope (Olympus, U-RFL-T).

The impact of PS-NPs on reproduction and larval development was determined in N_2 synchronized worms at the L4 larval stage that were fed PS-NPs at concentrations of 2.5 and 10 μg ml^{-1}, as described before. Two hours after the treatment, worms were singly plated on NGM-agar plates seeded with *E. coli* OP50, and the number of eggs laid by each worm was counted every day until the worm stopped laying. The larval development of the eggs laid in these experimental conditions was monitored daily until the adult stage by counting the number of worms at the different larval stages as described in the literature.[21] The effect of positive and negative PS-NPs on pharyngeal function and locomotor activity was assessed in synchronized worms at the L4 larval stage fed 2.5–10 μg ml^{-1} PS-NPs as already reported.[22,23] The pharyngeal pumping rate was measured by counting the number of times the terminal bulb of the pharynx contracted in 1 minute (pumps per min). To measure the locomotor activity, worms were picked up and transferred into a well of a 96-well ELISA plate containing 100 μl of 10 mM PBS, pH

7.4, and their motility was evaluated by counting the number of left–right movements in 1 minute (body bends per min).

2.7 Statistical analysis

Statistical analyses were performed using Prism GraphPad software v. 9.4 (GraphPad Software, San Diego, CA, USA). All data points were included, except for experiments where negative and/or positive controls did not give the expected outcome. No test for outliers was performed. Data were analyzed using one-way ANOVA corrected by a Bonferroni *post hoc* test, and the results were expressed as means ± SD or SEM. A *p*-value less than 0.05 was considered significant.

3. Results

3.1 NPs characterization

The amine-modified and carboxylate-modified, rhodamine-labeled fluorescent PS-NPs were characterized before being used for *in vitro* and *in vivo* studies. To this end, NPs were suspended in water, and the analyses were performed at room temperature. Results from DLS analysis indicated that the diameter of amine-modified PS-NPs ranged from ~20 nm up to 1 μm with a mean

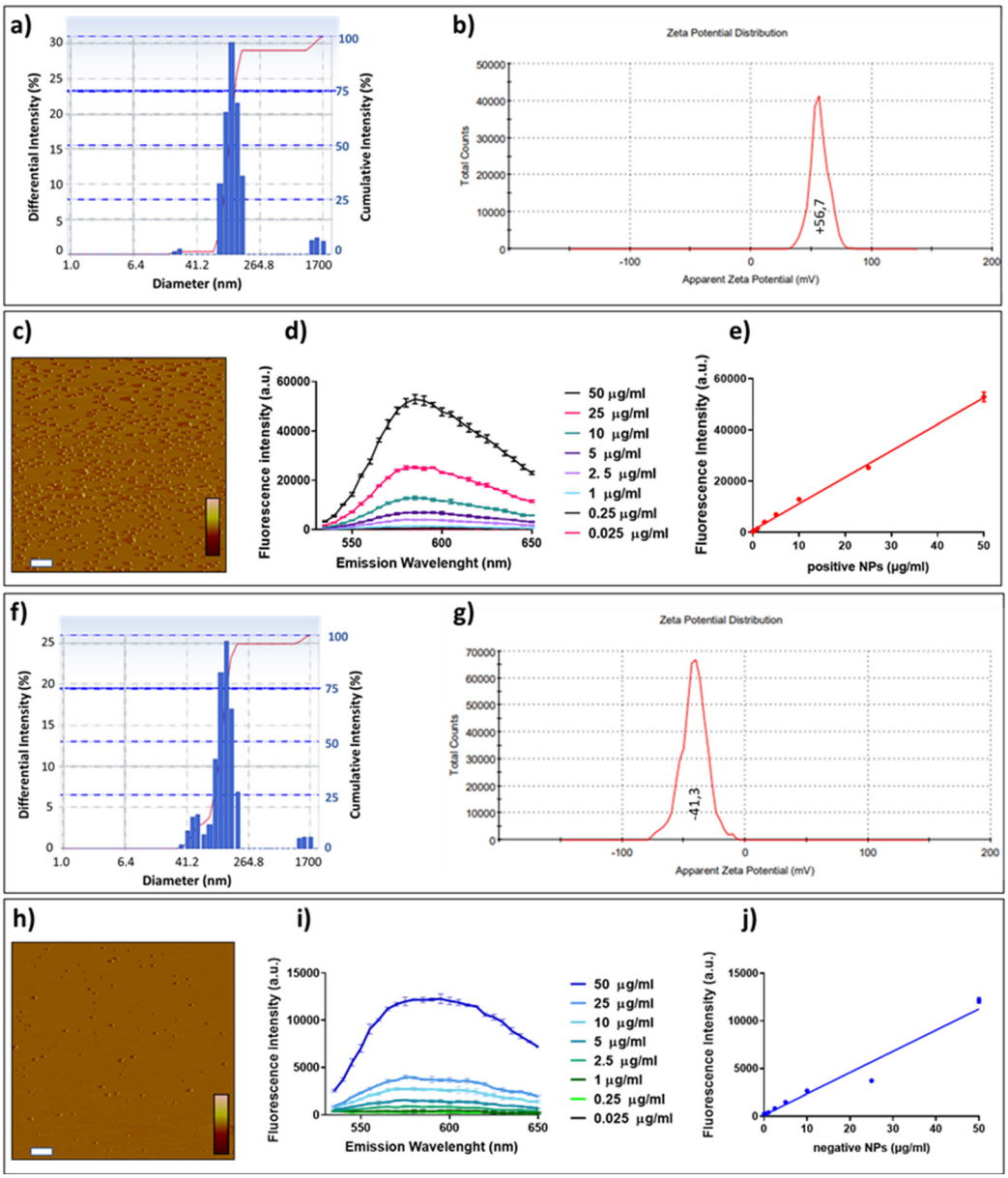

Fig. 1 Characterization of amine-modified (positive) and carboxylate-modified (negative) PS-NPs. a and f) Size distribution measured by DLS and b and g) the z-potential. c and h) Atomic force microscopy analysis obtained in phase mode. Scale bar = 1 μm, color scale: 0–150 mV. d and i) Fluorescence intensity spectra obtained with increasing concentrations of NPs. Data are mean ± SD. e and j) Correlation between the fluorescence intensity value registered at λ = 585 nm and the NPs concentration.

nominal diameter of 113 nm (Fig. 1a). Carboxylate-modified PS-NPs had diameters ranging from ~40 nm up to 1.7 μm with a mean nominal diameter of 130 nm (Fig. 1f). Analysis conducted on the same suspensions to determine the surface charge of NPs indicated a z-potential of +56.7 mV and −41.3 mV for amine-modified and carboxylate-modified NPs, respectively (Fig. 1b and g). Based on these data, we defined amine-modified PS-NPs as "positive" and carboxylate-modified PS-NPs as "negative." Topographical images of NPs surfaces obtained from AFM indicated that positive and negative PS-NPs were similarly monodispersed and had comparable spherical shapes (Fig. 1c and h).

Fluorometric spectra were also recorded to determine the maximum wavelength of NP emission and the concentration range in which a linear response occurred. Positive and negative PS-NPs suspended in water at increasing concentrations (0.025–50 μg ml^{-1}) exerted the maximal fluorescent emission at 585 nm (Fig. 1d and i). The fluorescence intensity recorded for negative PS-NPs was lower than the positive at all concentrations considered. This was attributable to negative NPs containing three-fold lower fluorophore concentration than positive ones, as the manufacturer's datasheet specified. As shown in Fig. 1e and j, a linear correlation between the concentration and the fluorescence intensity was observed for positive (R^2 = 0.99) and negative (R^2 = 0.96) PS-NPs.

3.2 Surface charge of NPs affected their cellular toxicity and internalization

In vitro studies were carried out to investigate the effect of positive and negative PS-NPs on cell growth, viability, and metabolic activity. HEK 293 cells were treated with different concentrations (2.5–25 μg ml^{-1}) of NPs, and their growth was monitored over time. Treatment with 25 μg ml^{-1} of positive NPs caused a significant reduction in the number of cells starting from 6 hours of incubation, while at the concentration of 2.5 and 10 μg ml^{-1}, they significantly affected the number of cells only at 72 hours (Fig. 2a). Thirty minutes after the treatment of cells with positive PS-NPs, a significant reduction of cell metabolic activity was observed only at 10 μg ml^{-1}. After 6 hours, both concentrations caused the maximum decrease in viability (Fig. 2c).

In contrast, no significant effect was observed with negative PS-NPs, even at the highest concentration of 10 μg ml^{-1} (Fig. 2d). These data indicate that the surface charge of PS-NPs affects the cell growth and viability and cell metabolic activity in HEK 293 cells. Once we selected the non-toxic concentration of 2.5 μg ml^{-1} for cell treatment, we moved to the study of cellular internalization. Representative pictures of the uptake of positive PS-NPs in HEK 293 cells are reported in Fig. 3a, and a time-lapse video is included in Video S1.† In this condition, at a concentration not inducing cytotoxicity, both parameters (dose and incubation time) affect the amount of signal inside the cells. Although the progressive increase of fluorescence inside the cells, furthermore confirmed by the quantitative analysis reported in Fig. 3b, the staining remained confined to the cytoplasmic region and did not overlap with the nuclear area (blue signal). On the other hand, as shown in Fig. 3c, negative PS-NPs had a lower internalization rate over time than positively charged ones (time-lapse screenshots and images are shown in ESI† Fig. S1 and S2). Images in Fig. 3d represent positive PS-NP

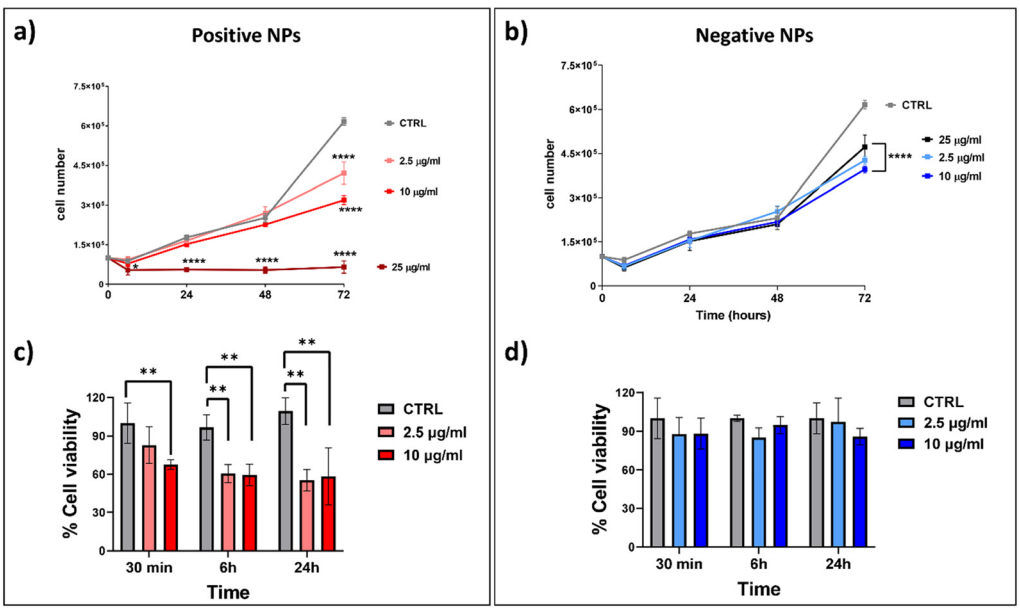

Fig. 2 Effect of positive and negative PS-NPs on cell growth and viability. Impact of different concentrations of a) positive and b) negative PS-NPs on cell growth of HEK 293 cells. Control cells (CTRL) were treated with medium alone. Data are the mean ± SD (N = 5). *$p < 0.1$ and ****$p < 0.001$ *vs.* CTRL at the same time-point according to one-way ANOVA and Bonferroni's *post hoc* test. Effect of c) positively charged and d) negatively charged PS-NPs (2.5 and 10 μg ml^{-1}) on cell viability of HEK 293 cells, determined by MTT, 30 minutes, 6 hours, and 24 hours after the treatment. Control cells (CTRL) were treated with medium alone. Data are the mean ± SD (N = 5). **$p < 0.01$ *vs.* CTRL at the same time-point according to one-way ANOVA and Bonferroni's *post hoc* test.

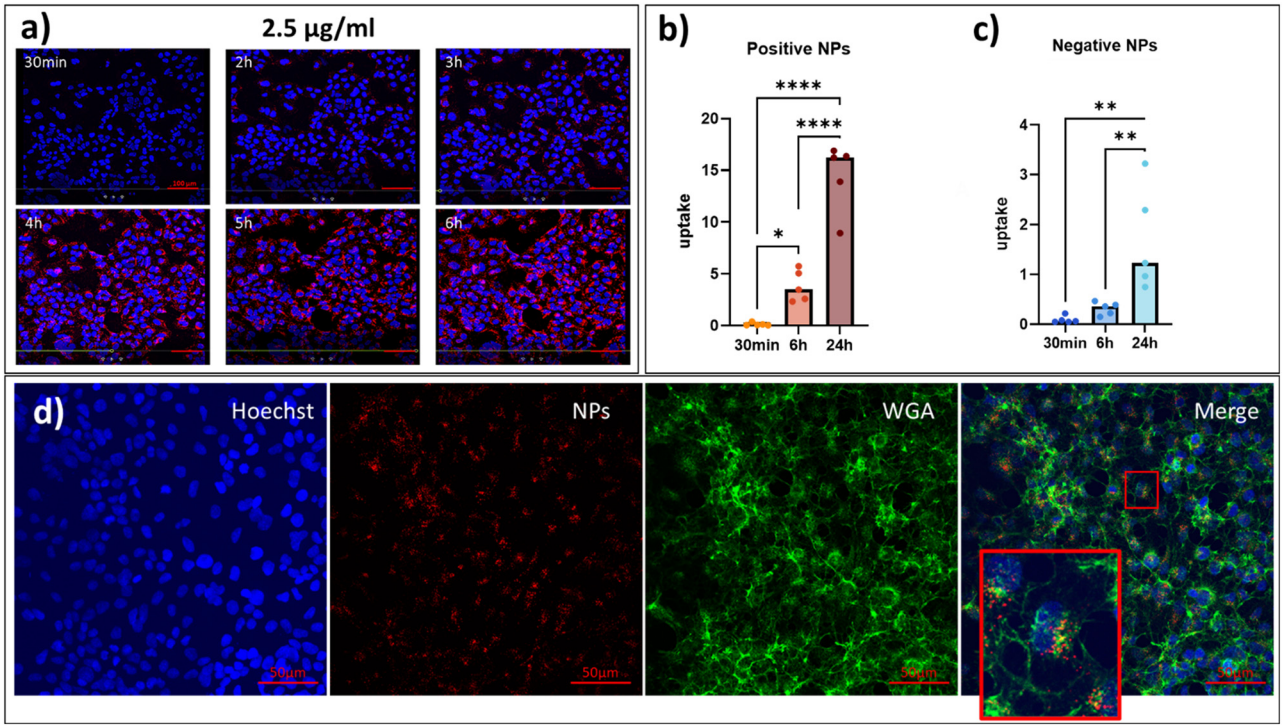

Fig. 3 Internalization pathway of positive PS-NPs and intracellular sub-localization. a) Representative screenshots of the time-lapse images of HEK 293 cells treated with 2.5 µg ml^{-1} positive PS-NPs (magnification 20×). Blue: Hoechst stained nuclei. Red: fluorescently labeled NPs. Scale bar: 100 µm. b and c) Quantification of the uptake of b) positive and c) negative NPs into HEK 293 cells at 30 minutes, 6, and 24 hours after the treatment. Data are the mean ± SD. *$p < 0.1$ **$p < 0.01$ and ****$p < 0.0001$ according to one-way ANOVA and Tukey *post hoc* test analysis. d) Split channels of a confocal image of HEK 293 cells treated with positive PS-NPs for 24 hours and the merged image indicating the typical spot-like distribution of PS-NPs into the cells. In the red square, a cell at a higher magnification highlights the subcellular localization of the NPs. Scale bar: 50 µm.

distribution in the cells. From left to right, split channels of the same image acquired at a confocal microscope are shown to underline the sub-localization of PS-NPs in cells 24 hours after treatment. In particular, at this time point, a higher density of NPs in the perinuclear area of the cells was visible. Also, from 30 minutes to 24 hours of treatment, PS-NPs gradually got closer to the nuclei of HEK 293 cells (ESI† Fig. S3) after cellular uptake. Indeed, exogenous material of various origins accumulated in the perinuclear region, possibly promoted by cytoskeleton dynamics.[24] The distribution and the size of the material suggested that each spot referred to a clusterization in endoplasmic vesicles, as indicated by the results shown in Fig. 4 (lower panel). These vesicles were confined to the cell body and were in tight connection with the cell-trafficking transport chain that stems from the plasma membrane and stops at the border of the nuclear membrane. The NP's ability to be uptaken from target cells is due to the interaction between the plasma membrane and the external charge of the NP. However, this is a necessary but not sufficient condition for the cell penetration. It is widely known that nanometric bodies exploit their typical dimension to activate the membrane budding and start the endocytic process in a so-called "trojan horse" phenomenon.[25]

To better understand the downstream process of the NP-membrane interaction and the budding formation, we used chlorpromazine as a selective inhibitor for clathrin-mediated endocytosis. This cationic amphiphilic drug causes clathrin to be sequestered in late endosomes, inhibiting coated pit endocytosis.[26] The pre-incubation of cells with chlorpromazine modified the uptake of PS-NPs (Fig. 4, upper panel). Two hours after the treatment, positive PS-NPs were internalized and localized in the cytoplasm, with their typical spot-like distribution; instead, in cells pre-treated with chlorpromazine, few particles were present inside the cytoplasm, and some others were still interacting with the cell membrane. An accumulation of the red signal to the periphery of cells was probably due to the electrochemical attraction between the positive surface of PS-NPs and the net anionic charge of the cell membrane. Still, chlorpromazine avoids their entrance into the cells. The presence, despite the inhibitor, of some NPs in the cells can be due to other mechanisms involved in the internalization and endocytosis exploited by the cells beyond the clathrin-mediated one, such as macropinocytosis, caveolae-dependent or independent endocytosis.[27] As shown in Fig. 4c, the inhibitor alone caused a two-fold reduction of cellular internalization of positive PS-NPs. By contrast, negatively charged PS-NPs at 2 hours of incubation haven't been internalized yet, this is why no difference could be observed between control cells and treated ones (ESI† Fig. S4). The close relationship between the vesicle-mediated endocytosis and the cellular fate of PS-NPs was confirmed by colocalization studies

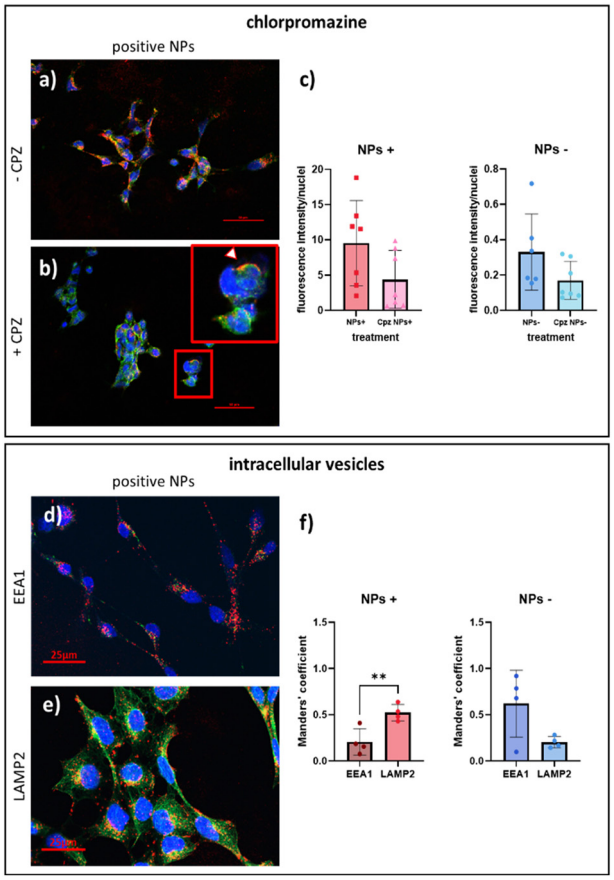

Fig. 4 Clathrin-mediated internalization pathway and intracellular fate of PS-NPs. Upper panel) Effect of chlorpromazine. Positive PS-NPs were administered for 2 hours to HEK 293 cells, a) not pre-treated (−CPZ) or b) pre-treated (+CPZ) for 30 minutes with chlorpromazine (CPZ) to investigate the clathrin-mediated internalization pathway. In the red square in b, a higher magnification of a cell showing the NPs sticking to the plasma membrane was shown. Blue: nuclei; red: PS-NPs; green: cell membranes. Scale bar: 50 μm. c) Quantification of NPs uptake in cells pre-treated or not with chlorpromazine before being exposed for 2 hours to positive or negative PS-NPs. Data are the mean ± SD. Lower panel) Vesicle-mediated endocytosis. Representative confocal images of cells treated with positive PS-NPs and stained with d) early endosome antigen-1 (EEA1) or e) lysosome-associated membrane protein-2 (LAMP2). Blue: nuclei; red: PS-NPs; green: intracellular vesicles. Scale bar: 25 μm. f) Pearson's coefficient of positive and negative PS-NPs with the vesicles. Data are the mean ± SD. $^{**}p = 0.0877$, unpaired *t*-test.

performed using antibodies directed against the early endosomes (EAA1) and the mature lysosomes (LAMP2), respectively (Fig. 4, lower panel).

The colocalization coefficient in the present case is related to the rate of NPs localized into the intracellular vesicle. A marked colocalization between vesicular staining and the signal associated with PS-NPs is evident. In Fig. 4d and e, vesicles are labeled in green, and PS-NPs are in red; the yellow spots represent the colocalization of the green and the red signals. The quantification of the index of co-localization of PS-NPs with the two markers, performed at the 24 hours of incubation, was expressed as Pearson's coefficient. This value simply describes the amount of overlap between two channels, *i.e.*, how much of the localization in one channel overlaps the localization in the other one and *vice versa*.[28] After 24 hours of incubation with the positive NPs, the colocalization coefficient results two-fold higher for lysosomal markers (LAMP2) compared to early endosomes (EEA1), thus indicating that, at that time point, positive PS-NPs had already proceeded toward the lysosomal pathway (Fig. 4e and f). Consistently with the data obtained in the internalization studies of negative PS-NPs, also for the colocalization, a slower intracellular pathway is shown, with a three-fold higher colocalization with early endosomes, rather than lysosomes. This could be explained both because the uptake is slower in terms of time, the intracellular and vesicular pathways, and because the negative particles are less likely to be internalized by HEK 293 cells (Fig. 4f).

3.3 Impact of protein corona on PS-NP uptake

Interaction with different biological fluids can play a pivotal role in the cellular uptake of NPs. We recently demonstrated intestinal villi efficiently adsorb ingested polymeric NPs and can reach filter organs moving from the bloodstream.[29] For this reason, we have focused our attention on the possible role of serum pre-incubation in PS-NP uptake.

Fig. 5 shows the internalization of positively charged PS-NPs in HEK 293 cells without or pre-incubating the NPs for 1

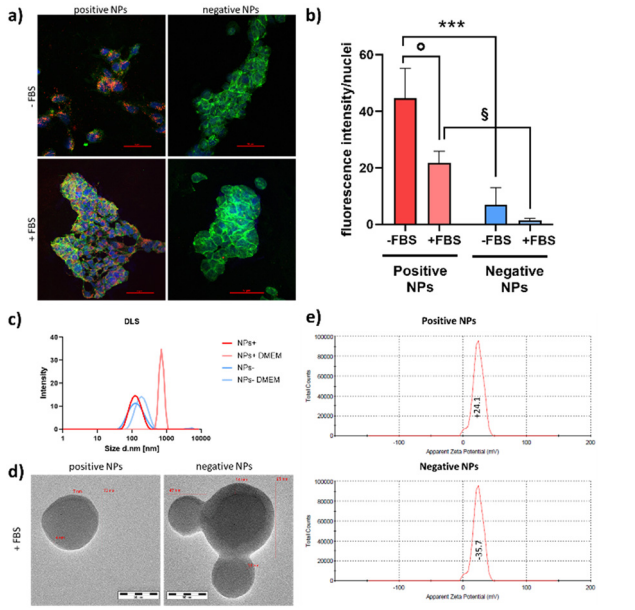

Fig. 5 Impact of protein corona on cellular uptake of PS-NPs. a) Representative confocal images of HEK 293 cells treated with PS-NPs not incubated or pre-incubated with FBS for 24 hours. Blue: nuclei; red: NPs; green: plasma membranes. Scale bar: 50 μm. b) Quantification of NPs cell uptake. Data are the mean ± SD. $^{\circ}p < 0.05$, $^{\S}p < 0.05$ and $^{***}p < 0.001$, one-way ANOVA and Bonferroni's *post hoc* test. c) DLS analysis and impact of the formation of the protein corona on the hydrodynamic diameter of the NPs. d) TEM images and measures of protein corona and diameter of positive and negative PS-NPs incubated 1 hour in FBS. e) Z-potential of positive and negative PS-NPs incubated 1 hour in FBS.

hour with 10% of FBS. Whereas the kinetic internalization of positive PS-NPs at basal condition was confirmed (− serum, Fig. 5a), the uptake was reduced when NPs were previously exposed to serum proteins. Such behavior could be explained by the binding to the external surface of NPs of negatively charged proteins to form the widely known process of protein corona. The decreased z-potential of positively charged PS-NPs in the presence of serum (Fig. 5e) reduced internalization. Also, in the case of negatively charged PS-NPs, a variation in the uptake after the incubation in serum can be observed. However, the uptake of the particles after 24 hours under basal conditions was already very low, and no significant difference was observed for the NPs pre-treated with serum (Fig. 5a and b).

The physical generation of protein corona after incubation in FBS was also confirmed by DLS analysis, where, in the presence of serum, both in case of positive and negative NPs, an increase in the hydrodynamic diameter can be observed (Fig. 5c). Then, TEM analysis to visualize the corona (Fig. 5d) and an SDS-PAGE to isolate the protein adsorbed on the NPs were carried out (ESI† Fig. S5) As shown in Fig. 5e, the presence of serum proteins drastically modified the surface charge of PS-NPs. Quite interestingly, this process occurred in both positive and negative PS-NPs. The corona formation did not modify the morphological features of NPs exclusively. Still, it changed their z-potential, which dropped from +56.7 mV to +24.1 mV for positively charged PS-NPs and slightly increased that of negatively charged PS-NPs from −41.3 mV to −35.7 mV (Fig. 5e). This characterization confirms that the incubation in serum exerts a key role in impairing the uptake of PS-NPs by HEK 293 cells. However, this effect cannot be exclusively ascribed to the change of z-potential but allegedly also to the nature of the adsorbed corona proteins,[30] as revealed by the decrease of uptake occurring in cells treated with negative PS-NPs.

3.4 Effect of surface charge on the toxicity of NPs *in vivo*

To investigate whether the different abilities of positive and negative PS-NPs to enter the cells and exert toxicity *in vitro* can also occur *in vivo*, their acute toxicity was evaluated in *C. elegans* through different behavioral assays. This worm has already been employed as a model organism to study the fate of ingested PS-NPs, showing that they mainly accumulate in the worms' gut.[31–33] Accordingly, in our experimental conditions, the administration to worms for 2 hours of both positive and negative PS-NPs (10 μg ml^{-1}) in the absence of *E. coli* OP50 resulted in a similar distribution of NPs in worms, mainly located in the intestine (Fig. 6).

In addition, it was reported that the long-term exposure of worms to different PS-NPs led to defects in reproduction, development, and locomotion.[32,33] We here investigated whether a single administration to *C. elegans* of PS-NPs with different z-potentials can affect worms' behaviors known to be modified by toxic compounds, like viability, reproduction, development, pharyngeal activity, and motility. To this end,

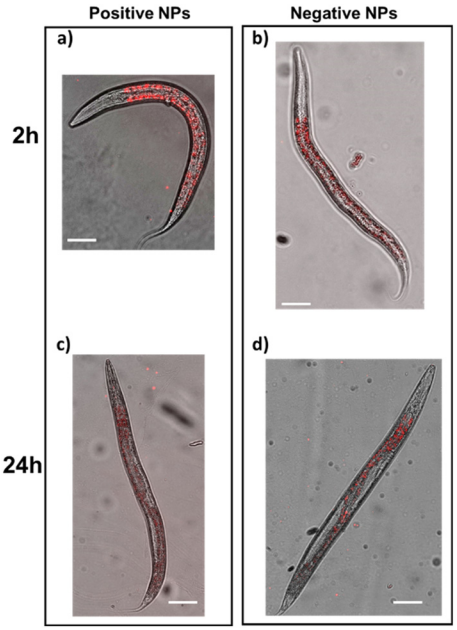

Fig. 6 Positive and negative PS-NPs have the same distribution in *C. elegans*. Worms (100 worms per 100 μl) were fed for 2 hours 10 μg ml^{-1} positive or negative PS-NPs suspended in 10 mM PBS, pH 7.4 in the absence of OP50 *E. coli*, then plated on NGM plates seeded with the bacteria. a–d) Representative images of worms taken a and b) 2 hours and c and d) 24 hours after treatment. Images show overlays of red fluorescence signal of PS-NPs and light microscopy. Scale bar: 50 μm.

synchronized worms on the L4 larval stage were fed with increasing concentrations of positive and negative PS-NPs (0.5–50 μg ml^{-1}), and the number of viable worms was scored 24 hours later. Control worms were treated with the same volume of 10 mM PBS, pH 7.4 (vehicle). Feeding worms with positive but not negative PS-NPs caused a dose-dependent reduction of their viability, with a half-maximal inhibitory concentration (IC_{50}) of 11.79 μg ml^{-1} (Fig. 7a and b).

The effect of PS-NPs on worms' feeding behaviour and motility was evaluated. The pharyngeal activity of worms fed 2.5 and 10 μg ml^{-1} positive PS-NPs, determined 2 hours after their plating, was 8.5% and 17.4% lower than controls, respectively (Fig. 7c). This dysfunction was partially recovered after 24 hours since no significant effect was seen with 2.5 μg ml^{-1}. A 7.8% reduction was observed with 10 μg ml^{-1} (Fig. 7d). Positive NPs also caused a decrease in worms' motility, expressed as body bends per minute, which worsened with time. At 2 hours, only worms fed 10 μg ml^{-1} exerted a significant reduction of the number of body bends, which was 12.5% lower than controls (Fig. 7e). At 24 hours, the motility was 14.9% and 16.7% lower than controls, in worms treated with 2.5 and 10 μg ml^{-1} NPs, respectively (Fig. 7f). No modification of the pumping rate and motility was observed in worms treated with negative PS-NPs (Fig. 7c–f).

We then evaluated whether feeding worms with PS-NPs, even at non-toxic concentrations (2.5 and 10 μg ml^{-1}), could modify their reproductive capacity, determined by the overall number of eggs laid during their life. Neither positive nor

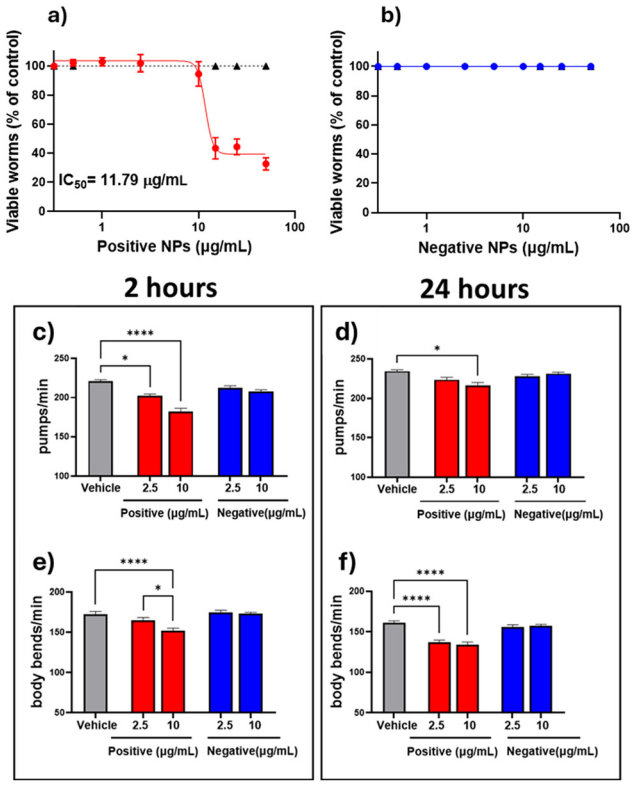

Fig. 7 Acute effect of PS-NPs on the viability, pharyngeal function, and motility. Worms (100 worms per 100 µl) were fed for 2 hours with 0.5–50 µg ml^{-1} of positive and negative PS-NPs suspended in 10 mM PBS, pH 7.4 in the absence of OP50 *E. coli*, then plated on NGM plates seeded with the bacteria. Control worms were fed only 10 mM PBS, pH 7.4 (vehicle). The number of viable worms fed a) positive and b) negative PS-NPs was evaluated 24 h later and expressed as a percentage of the control. The black line in a) represents the control worms. Data are the mean ± SEM (N = 5). c and d) The pharyngeal activity was determined c) 2 and d) 24 hours after plating by measuring the number of pharyngeal bulb contractions per minute (pumps per min). Data are mean ± SEM (N = 30 worms per group). e and f) The locomotor activity was recorded e) 2 and f) 24 hours after plating (body bends per min). Data are mean ± SEM (N = 24 worms per group). *$p < 0.05$ and ****$p < 0.001$ *vs.* vehicle, one-way ANOVA, Bonferroni's *post hoc* analysis of nematodes.

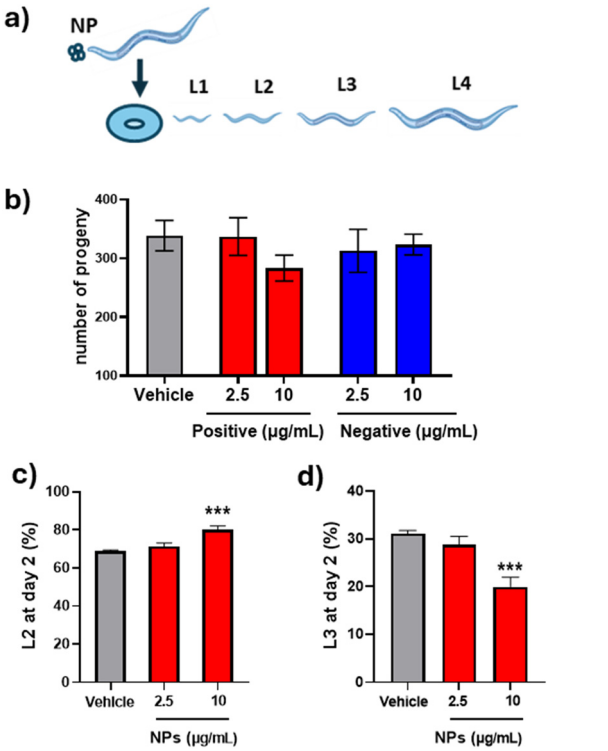

Fig. 8 Effect of PS-NPs on the reproduction and development of nematodes. a) Schematic representation of the experiments performed to evaluate the effect of NPs on the reproduction and development of worms. Created with **https://BioRender.com**. Worms (100 worms per 100 µl) were fed for 2 hours with 2.5 µg ml^{-1} or 10 µg ml^{-1} of positive and negative PS-NPs suspended in 10 mM PBS, pH 7.4, in the absence of OP50 *E. coli*, then plated on NGM plates seeded with the bacteria. Control worms were fed only 10 mM PBS, pH 7.4 (vehicle). b) The number of progenies after plating was scored. Mean ± SEM (N = 5 worms per group). Percentage of worms at c) L2 and d) L3 larval stage two days after egg hatching. The mean ± SEM (N = 10 worms per group). ***$p < 0.005$ *vs.* vehicle, one-way ANOVA, and Bonferroni's *post hoc* test.

negative PS-NPs, at all the concentrations tested, caused a significant reduction in progeny (Fig. 8a and b). However, when the larval growth of nematodes was evaluated, a significant effect was observed only on the progeny generated by worms fed 10 µg ml^{-1} positive NPs (ESI† Fig. S6) with a significantly higher percentage of worms at the L2 larval stage (Fig. 8c) and a lower percentage in the L3 larval stage (Fig. 8d) compared to control worms. No effect was observed on the larval development of the progeny generated by nematodes fed negative PS-NPs.

These findings indicate that the acute treatment of *C. elegans* with positively charged PS-NPs can specifically affect their viability. In addition, at doses that did not modify the viability of worms, positive PS-NPs can also exert a sub-toxic effect, causing an alteration of normal development, an impairment in feeding behaviour, and a defect in motility.

4. Discussion

The chemical nature of plastic and its effects on animal and environmental health have been debated since the last century. Although the main actions aimed at limiting the harmfulness of plastics have focused on their macroscopic dimension and have been devoted to the problem of their degradation, a growing body of evidence revealed that physico-chemical factors cannot be neglected.[34,35]

The degradative process of microplastics does not remove the hazard because it leads to the formation of micrometric and nanometric fragments that can interact with biological matrices. It is universally known that almost all solid bodies ranging from a few to 400 nm can interact with different biological matrices (*e.g.*, biological fluids, cells, organs, systems, and entire bodies) in a different way documented on a macroscopic scale.[36,37] In particular, the mechanism of entry in cells by a mechanism universally defined as the "Trojan horse effect" represents a stereotyped phenomenon characterizing the bio-nano interaction.[38]

Although all nanomaterials share the ability to penetrate inside the cells, it is also well documented that little variations in their physico-chemical properties may induce great variations in the rate of internalization.[39] For almost all nanomaterials, including NPs, their size, shape, surface charge, degree of stability, and rigidity can significantly influence their ability to penetrate host tissues and cells and to determine the processes degradation, clearance, their reactivity with endogenous interactors (*e.g.*, oxidative stress, modification of organization of vesicular structures, energy deficits or activation of pro-apoptotic pathways).[40]

In recent years, several *in vitro* and *in vivo* studies have highlighted the role of the physico-chemical parameters in plastic nanosafety.[41,42] One study aimed at comparing two types of NPs with different levels of biodegradability, poly-caprolactone and polylactic acid (PLA)-8, on human MDA-MB 231.1833 and mouse 4T1 triple-negative breast cancer cell lines. Importantly, the material was the only element differentiating the two NPs, whereas size, shape, surface charge potential, and the surfactant used to maintain the colloidal stability were similar. The internalization results demonstrated a strong influence of the stiffness on the penetration capacity. In particular, it was observed that the limiting factor for the uptake of the NPs with the "softer" material (PLA-8-NPs) was not related to a lower capacity to interact with the plasma membrane but rather to difficulty in generating the process of membrane deformation required for the budding and the endocytotic vesicle formation.[8]

The use of PLA can have a somewhat limited impact on an overall policy program aimed at driving the formation of guidelines for safe and sustainable plastic industrial production. However, remembering that its use is confined to the dermocosmesis and extends to other fields, such as the agronomic sector, is useful. This application also plays a role in animal and human health. It is known that the propagation of NPs from soil to air allows them to interact with the host through ingestion and inhalation. Although PS has different features concerning PLA, both in terms of rigidity and biodegradability, the present work confirms the formation of the endocytotic vesicle for the penetration of NPs into the host cell. It is clear from our result that the inhibition of the clathrin coating through the use of the specific inhibitor chlorpromazine induces a scenario very similar to that which we had documented in the work with PLA-8, in which an assembly of NPs, highlighted by the intense red signal associated with the fluorophore, it is observable to delineate the external contours of the cellular membrane. Material is not the only parameter that influences interaction with living systems. In a further similar study, the role of the size and the surface charge on the entry of polymethylmethacrylate (PMMA) NP in the MDA-MB 231.1833 and 4T1 cell lines was investigated by keeping the shape fixed.[7]

Similarly to what was obtained with PS-NPs, a marked difference related to the surface charge (z-potential) was observed. At the same time, the effect of the size, the diameter of the nanoplates varied from 50 to 200 nm, did not have a significant impact. PMMA was chosen for its huge, large-scale production since it is used in various sectors such as construction, transport, lighting, and automotive. For both PMMA and PS-NPs, the entry inside the cytoplasm was markedly lower in cells incubated with negatively charged particles independently on both the material and the cell target. However, unlike the process observed for PLA-8, the negative z-potential did not influence the mechanism of endocytotic vesicle formation but was due to the electrostatic charge repulsion between NPs and the outer plasma membrane.[43,44] Although fewer, the fluorescent spots observed in cells incubated with negatively charged PS-NPs were similar to those found after treatment with positively charged ones, and no accumulation of fluorescent agglomerates in the peripheral border of cells was detected. Once internalized, the vesicular transport occurs independently of the charge, as demonstrated by the progressive reduction of the distance to the nucleus of the signal associated with both positive and negative PS-NPs.

As expected, PS-NPs penetrated HEK 293 cells and moved to the perinuclear area by the classical retrograde vesicular transport, as demonstrated by our co-localization experiments between the NPs signal and the main markers of early, late endosomes and lysosomes. Despite a strong entrapment in intracellular vesicles, the measurement of the coefficient of co-localization, together with the presence of red spots not colocalizing with the three markers, suggest that a low amount of PS-NPs can freely circulate into the cytosol. In agreement with this hypothesis, a recent study performed in mouse embryonic fibroblasts demonstrated that PS-NPs could migrate into the cytoplasm, likely by endosomal escape.[45]

Not only are intrinsic properties responsible for the fate of NPs, but the ecological and biological environments may also play a key role. The interplay between PS-NPs and biological fluids is extremely relevant among the different factors. According to previous studies carried out with PS-NPs[46] in the present study, we found that the pre-incubation of PS-NPs with serum reduced the penetration of positively charged PS-NPs inside HEK293 cells. This effect was not unexpected because it has been widely documented for many types of NPs, in particular those with a spherical geometry and a positive surface charge, which can bind proteins in a gradual and progressive process better known as protein corona formation.[47] The formation of the protein corona can inhibit the uptake of NPs through two different mechanisms: a) in the case of ligand-mediated internalization processes, which more commonly occurs in the case of functionalized nanocarriers associated with drugs or siRNAs, the corona can mask the binding site thus reducing its selectivity and affinity;[48] b) in the most common case for many nanomaterials, including plastics, the reduced penetration is mediated by a significant reduction in electrostatic attraction as the proteins bound to the surface of the NP have a net negative charge and could mask the original charge of the particles.

The study of pre-incubation in serum not only represents a tool to confirm the role of surface in cell entry but also has an important practical impact. It is well known that NPs can be absorbed into the bloodstream after ingestion and inhalation, migrate inside the organs, and penetrate cells. Therefore, the effect of the serum coating may reduce the difference in interaction with host cells compared to the *in vitro* condition.

In the previous study performed with the PMMA NPs we found that those positively charged induced a concentration-dependent and time-dependent significant reduction of the cell number in both MDA-MB 231.1833 and 4T1 cells. Our study confirmed the role played by the external surface and the incubation time on the cell number.

All these observations highlighted the possible relevance of the z-potential in bio-nano interaction and nanosafety. However, *in vitro* analysis is always limited, and models with a more complex biological organization are strongly needed to confirm this preliminary evidence. To this end, our study was extended to the nematode *C. elegans*, evaluating whether PS-NPs may exert a toxic effect and can be related to their external charge.

Jiang *et al.*[31] first investigated the influence of surface charges on long-term PS-NPs toxicity in *C. elegans*, showing that positively charged NPs adversely affected the growth and development of worms without impacting their lifespan.[49] Our data confirmed for the first time that positive, but not negative PS-NPs, specifically caused dose-dependent acute and sub-acute toxic effects. Even after a sub-toxic dose, positive PS-NPs impact normal worm larval development,[50–52] but do not affect worms' viability. This effect can be ascribed to the ability of NPs to enter the egg cell, thus affecting its subsequent cellular divisions and development, or to unknown epigenetic modifications. We also demonstrated that positively charged PS-NPs can significantly reduce pharyngeal contraction, a behavior commonly adopted by *C. elegans* as a defensive response to chemical stressors.[53] A detrimental effect on worm locomotion, which persisted over time, was also observed as an indication of the onset of a dose- and time-dependent neuromuscular dysfunction.

The mechanisms underlying the defects caused by the acute administration of positive PS-NPs are still unclear. Previous findings suggest that they may have the ability to induce oxidative stress and metabolic alterations,[54] which may contribute to both pharyngeal and locomotion dysfunctions. In particular, it has been reported that PS-NPs cause a decrease in glutamic acid, the substrate for γ-aminobutyric acid, one of the primary neurotransmitters involved in movement regulation in *C. elegans.*[55]

5. Conclusions

The present study stems from a previous body of evidence reporting a clear size-dependent interaction between fluorescently labeled polystyrene nanoparticles and mammalian cells,[56] such as cytotoxic effects influenced by their size and z potential.[57] A combined analysis confirming a clear relationship between MNPs accumulation and toxicity is highlighted here in cells and animals. The effect of positively charged PS-NPs in cells and worms is likely due to the z-potential rather than the amount of their accumulation. These results provide valuable insights into the role of every single physico-chemical parameter on the potential health risks associated with NP pollution. In addition, this study could be supportive for development of harmonized standard guidelines (*i.e.*, OECD, ISO and CEN) and regulatory guidance (*e.g.*, REACH, Biocides, Consumer Products, Food and Feed, Medical Technologies) to reduce plastic production, stop environmental degradation, and protect the health of living organisms.

Data availability

Data for this article are available at Zenodo under request to the corresponding authors.

Author contributions

Conceptualization, P. B., and L. D.; investigation, G. Y. M., C. N., M. I., A. M., L. R., N. B., A. C., A. D. L., F. F., formal analysis, G. Y. M., C. N., L. S., D. P., G. C.; data curation, G. Y. M., C. N., P. B., L. D.; writing – original draft preparation, G. Y. M., C. N., P. B., L. D.; supervision, P. B., L. D.; funding acquisition, P. B., L. D. All authors have read and agreed to the published version of the manuscript.

Conflicts of interest

The authors declare no conflict of interest.

Acknowledgements

This research was funded by the European Union's Horizon Europe RESEARCH AND INNOVATION ACTIONS PROGRAMME, Project "Platform Optimisation to Enable Nanomaterial Safety Assessment for Rapid commercialization (POTENTIAL)", Grant number 101092901. This study was conducted under the Italian Institute for Planetary Health (IIPH) framework. We thank Dr. Alessandro Molinelli of the Department of Chemistry, Materials, and Chemical Engineering "Giulio Natta" Politecnico of Milan for his help in DLS and Z-potential experiments. *C. elegans* and OP50 *E. coli* were provided by the GCG, funded by NIH Office Research Infra Structure Programs (P40 OD010440). The Table of Contents and Fig. 8a were Created with **https://BioRender.com**.

Notes and references

1 *Plastics - The Facts 2017*, An analysis of European plastics production, demand and waste data, 2017, available from: **https://plasticseurope.org/wp-content/uploads/2021/10/2017-Plastics-the-facts.pdf**.
2 S. Ali, D. A. Bukhari and A. Rehman, Call for biotechnological approach to degrade plastic in the era of COVID-19 pandemic, *Saudi J. Biol. Sci.*, 2023, **30**(3), 103583.

3 K. Kik, B. Bukowska and P. Sicińska, Polystyrene nanoparticles: Sources, occurrence in the environment, distribution in tissues, accumulation and toxicity to various organisms, *Environ. Pollut.*, 2020, **262**, 114297.
4 Y. Tokiwa, B. Calabia, C. Ugwu and S. Aiba, Biodegradability of Plastics, *Int. J. Mol. Sci.*, 2009, **10**(9), 3722–3742.
5 Y. Ruan, Z. Zhong, X. Liu, Z. Li, J. Li and L. Sun, *et al.*, Correlation between cellular uptake and cytotoxicity of polystyrene micro/nanoplastics in HeLa cells: A size-dependent matter, *PLoS One*, 2023, **18**(8), e0289473.
6 A. Roshanzadeh, S. Park, S. E. Ganjbakhsh, J. Park, D. H. Lee and S. Lee, *et al.*, Surface Charge-Dependent Cytotoxicity of Plastic Nanoparticles in Alveolar Cells under Cyclic Stretches, *Nano Lett.*, 2020, **20**(10), 7168–7176.
7 L. Sitia, K. Paolella, M. Romano, M. B. Violatto, R. Ferrari and S. Fumagalli, *et al.*, An integrated approach for the systematic evaluation of polymeric nanoparticles in healthy and diseased organisms, *J. Nanopart. Res.*, 2014, **16**(7), 2481.
8 L. Sitia, R. Ferrari, M. B. Violatto, L. Talamini, L. Dragoni and C. Colombo, *et al.*, Fate of PLA and PCL-Based Polymeric Nanocarriers in Cellular and Animal Models of Triple-Negative Breast Cancer, *Biomacromolecules*, 2016, **17**(3), 744–755.
9 S. Lambert and M. Wagner, Characterisation of nanoplastics during the degradation of polystyrene, *Chemosphere*, 2016, **145**, 265–268.
10 A. Kurtz-Chalot, J. P. Klein, J. Pourchez, D. Boudard, V. Bin and O. Sabido, *et al.*, Quantification of nanoparticle endocytosis based on double fluorescent pH-sensitive nanoparticles, *Biomed. Microdevices*, 2015, **17**(2), 42.
11 S. K. Kloet, A. P. Walczak, J. Louisse, H. H. J. Van Den Berg, H. Bouwmeester and P. Tromp, *et al.*, Translocation of positively and negatively charged polystyrene nanoparticles in an in vitro placental model, *Toxicol. In Vitro*, 2015, **29**(7), 1701–1710.
12 Z. Li, T. Xu, L. Peng, X. Tang, Q. Chi and M. Li, *et al.*, Polystyrene nanoplastics aggravates lipopolysaccharide-induced apoptosis in mouse kidney cells by regulating IRE1/XBP1 endoplasmic reticulum stress pathway via oxidative stress, *J. Cell. Physiol.*, 2023, **238**(1), 151–164.
13 G. Sitia, F. Fiordaliso, M. B. Violatto, J. F. Alarcon, L. Talamini and A. Corbelli, *et al.*, Food-Grade Titanium Dioxide Induces Toxicity in the Nematode Caenorhabditis elegans and Acute Hepatic and Pulmonary Responses in Mice, *Nanomaterials*, 2022, **12**(10), 1669.
14 L. Frézal and M. A. Félix, C. elegans outside the Petri dish, *eLife*, 2015, **4**, e05849.
15 J. Van Den Hoogen, S. Geisen, D. Routh, H. Ferris, W. Traunspurger and D. A. Wardle, *et al.*, Soil nematode abundance and functional group composition at a global scale, *Nature*, 2019, **572**(7768), 194–198.
16 Q. Rui, Y. Zhao, Q. Wu, M. Tang and D. Wang, Biosafety assessment of titanium dioxide nanoparticles in acutely exposed nematode Caenorhabditis elegans with mutations of genes required for oxidative stress or stress response, *Chemosphere*, 2013, **93**(10), 2289–2296.
17 L. Iannarelli, A. M. Giovannozzi, F. Morelli, F. Viscotti, P. Bigini and V. Maurino, *et al.*, Shape engineered TiO_2 nanoparticles in Caenorhabditis elegans: a Raman imaging based approach to assist tissue-specific toxicological studies, *RSC Adv.*, 2016, **6**(74), 70501–70509.
18 H. Ma, K. A. Lenz, X. Gao, S. Li and L. K. Wallis, Comparative toxicity of a food additive TiO2, a bulk TiO2, and a nano-sized P25 to a model organism the nematode C. elegans, *Environ. Sci. Pollut. Res.*, 2019, **26**(4), 3556–3568.
19 C. Hu, J. Hou, Y. Zhu and D. Lin, Multigenerational exposure to TiO2 nanoparticles in soil stimulates stress resistance and longevity of survived C. elegans via activating insulin/IGF-like signaling, *Environ. Pollut.*, 2020, **263**, 114376.
20 M. Porta-de-la-Riva, L. Fontrodona, A. Villanueva and J. Cerón, Basic Caenorhabditis elegans Methods: Synchronization and Observation, *J. Visualized Exp.*, 2012(64), 4019.
21 L. Byerly, R. C. Cassada and R. L. Russell, The life cycle of the nematode Caenorhabditis elegans, *Dev. Biol.*, 1976, **51**(1), 23–33.
22 L. Diomede, P. Rognoni, F. Lavatelli, M. Romeo, E. Del Favero and L. Cantù, *et al.*, A Caenorhabditis elegans–based assay recognizes immunoglobulin light chains causing heart amyloidosis, *Blood*, 2014, **123**(23), 3543–3552.
23 F. Morelli, M. Romeo, M. M. Barzago, M. Bolis, D. Mattioni and G. Rossi, *et al.*, V363I and V363A mutated tau affect aggregation and neuronal dysfunction differently in C. elegans, *Neurobiol. Dis.*, 2018, **117**, 226–234.
24 I. Rivolta and M. Panariti, The effect of nanoparticle uptake on cellular behavior: disrupting or enabling functions?, *Nanotechnol., Sci. Appl.*, 2012, 87.
25 L. K. Limbach, P. Wick, P. Manser, R. N. Grass, A. Bruinink and W. J. Stark, Exposure of Engineered Nanoparticles to Human Lung Epithelial Cells: Influence of Chemical Composition and Catalytic Activity on Oxidative Stress, *Environ. Sci. Technol.*, 2007, **41**(11), 4158–4163.
26 S. Lai, K. Hida, S. Man, C. Chen, C. Machamer and T. Schroer, *et al.*, Privileged delivery of polymer nanoparticles to the perinuclear region of live cells via a non-clathrin, non-degradative pathway, *Biomaterials*, 2007, **28**(18), 2876–2884.
27 F. Zhao, Y. Zhao, Y. Liu, X. Chang, C. Chen and Y. Zhao, Cellular Uptake, Intracellular Trafficking, and Cytotoxicity of Nanomaterials, *Small*, 2011, **7**(10), 1322–1337.
28 Microscopy colocalization theoretical background, Huygens Imaging Academy Scientific Volume Imaging; available from: https://svi.nl/ColocalizationTheory.
29 L. Morelli, S. Gimondi, M. Sevieri, L. Salvioni, M. Guizzetti and B. Colzani, *et al.*, Monitoring the Fate of Orally Administered PLGA Nanoformulation for Local Delivery of Therapeutic Drugs, *Pharmaceutics*, 2019, **11**(12), 658.
30 M. Mahmoudi, M. P. Landry, A. Moore and R. Coreas, The protein corona from nanomedicine to environmental science, *Nat. Rev. Mater.*, 2023, **8**(7), 422–438.
31 W. Jiang, W. Yan, Q. Tan, Y. Xiao, Y. Shi and J. Lei, *et al.*, The toxic differentiation of micro- and nanoplastics verified by gene-edited fluorescent Caenorhabditis elegans, *Sci. Total Environ.*, 2023, **856**, 159058.

32 K. W. Kim, N. H. Tang, C. A. Piggott, M. G. Andrusiak, S. Park and M. Zhu, *et al.*, Expanded genetic screening in Caenorhabditis elegans identifies new regulators and an inhibitory role for NAD+ in axon regeneration, *eLife*, 2018, **7**, e39756.

33 Y. Qiu, Y. Liu, Y. Li, G. Li and D. Wang, Effect of chronic exposure to nanopolystyrene on nematode Caenorhabditis elegans, *Chemosphere*, 2020, **256**, 127172.

34 L. Talamini, M. B. Violatto, Q. Cai, M. P. Monopoli, K. Kantner and Ž. Krpetić, *et al.*, Influence of Size and Shape on the Anatomical Distribution of Endotoxin-Free Gold Nanoparticles, *ACS Nano*, 2017, **11**(6), 5519–5529.

35 J. Fernandez Alarcon, M. Soliman, T. U. Lüdtke, E. Clemente, M. Dobricic and M. B. Violatto, *et al.*, Long-term retention of gold nanoparticles in the liver is not affected by their physicochemical characteristics, *Nanoscale*, 2023, **15**(19), 8740–8753.

36 D. B. Chithrani, Intracellular uptake, transport, and processing of gold nanostructures, *Mol. Membr. Biol.*, 2010, **27**(7), 299–311.

37 C. M. Beddoes, C. P. Case and W. H. Briscoe, Understanding nanoparticle cellular entry: A physicochemical perspective, *Adv. Colloid Interface Sci.*, 2015, **218**, 48–68.

38 D. B. Chithrani, M. Dunne, J. Stewart, C. Allen and D. A. Jaffray, Cellular uptake and transport of gold nanoparticles incorporated in a liposomal carrier, *Nanomed.: Nanotechnol., Biol. Med.*, 2010, **6**(1), 161–169.

39 P. Ruenraroengsak, K. Aljamal, N. Hartell, K. Braeckmans, S. Desmedt and A. Florence, Cell uptake, cytoplasmic diffusion and nuclear access of a 6.5nm diameter dendrimer, *Int. J. Pharm.*, 2007, **331**(2), 215–219.

40 K. Remaut, B. Lucas, K. Braeckmans, J. Demeester and S. C. De Smedt, Pegylation of liposomes favours the endosomal degradation of the delivered phosphodiester oligonucleotides, *J. Controlled Release*, 2007, **117**(2), 256–266.

41 Y. He, J. Li, J. Chen, X. Miao, G. Li and Q. He, *et al.*, Cytotoxic effects of polystyrene nanoplastics with different surface functionalization on human HepG2 cells, *Sci. Total Environ.*, 2020, **723**, 138180.

42 M. B. Paul, V. Stock, J. Cara-Carmona, E. Lisicki, S. Shopova and V. Fessard, *et al.*, Micro- and nanoplastics – current state of knowledge with the focus on oral uptake and toxicity, *Nanoscale Adv.*, 2020, **2**(10), 4350–4367.

43 S. Jeon, J. Clavadetscher, D. K. Lee, S. Chankeshwara, M. Bradley and W. S. Cho, Surface Charge-Dependent Cellular Uptake of Polystyrene Nanoparticles, *Nanomaterials*, 2018, **8**(12), 1028.

44 E. Fröhlich, The role of surface charge in cellular uptake and cytotoxicity of medical nanoparticles, *Int. J. Nanomed.*, 2012, 5577.

45 S. W. Han, J. Choi and K. Y. Ryu, Stress Response of Mouse Embryonic Fibroblasts Exposed to Polystyrene Nanoplastics, *Int. J. Mol. Sci.*, 2021, **22**(4), 2094.

46 A. Salvati, C. Åberg, T. Dos Santos, J. Varela, P. Pinto and I. Lynch, *et al.*, Experimental and theoretical comparison of intracellular import of polymeric nanoparticles and small molecules: toward models of uptake kinetics, *Nanomed.: Nanotechnol., Biol. Med.*, 2011, **7**(6), 818–826.

47 T. Cedervall, I. Lynch, S. Lindman, T. Berggård, E. Thulin and H. Nilsson, *et al.*, Understanding the nanoparticle–protein corona using methods to quantify exchange rates and affinities of proteins for nanoparticles, *Proc. Natl. Acad. Sci. U. S. A.*, 2007, **104**(7), 2050–2055.

48 A. Salvati, A. S. Pitek, M. P. Monopoli, K. Prapainop, F. B. Bombelli and D. R. Hristov, *et al.*, Transferrin-functionalized nanoparticles lose their targeting capabilities when a biomolecule corona adsorbs on the surface, *Nat. Nanotechnol.*, 2013, **8**(2), 137–143.

49 Y. Shang, S. Wang, Y. Jin, W. Xue, Y. Zhong and H. Wang, *et al.*, Polystyrene nanoparticles induced neurodevelopmental toxicity in Caenorhabditis elegans through regulation of dpy-5 and rol-6, *Ecotoxicol. Environ. Saf.*, 2021, **222**, 112523.

50 S. W. Kim, D. Kim, S. W. Jeong and Y. J. An, Size-dependent effects of polystyrene plastic particles on the nematode Caenorhabditis elegans as related to soil physicochemical properties, *Environ. Pollut.*, 2020, **258**, 113740.

51 Y. Zhao, J. Chen, R. Wang, X. Pu and D. Wang, A review of transgenerational and multigenerational toxicology in the in vivo model animal *Caenorhabditis elegans*, *J. Appl. Toxicol.*, 2023, **43**(1), 122–145.

52 R. Xu, X. Hua, Q. Rui and D. Wang, Polystyrene nanoparticles cause dynamic alteration in mitochondrial unfolded protein response from parents to the offspring in C. elegans, *Chemosphere*, 2022, **308**, 136154.

53 D. Jones and E. P. M. Candido, Feeding is inhibited by sublethal concentrations of toxicants and by heat stress in the nematodeCaenorhabditis elegans: Relationship to the cellular stress response, *J. Exp. Zool.*, 1999, **284**(2), 147–157.

54 S. W. Kim, D. Kim, S. W. Jeong and Y. J. An, Size-dependent effects of polystyrene plastic particles on the nematode Caenorhabditis elegans as related to soil physicochemical properties, *Environ. Pollut.*, 2020, **258**, 113740.

55 E. M. Jorgensen, *WormBook The online review of C.elegans biology*, GABA, 2005, available from: **https://www.wormbook.org/chapters/www_gaba/gaba.html**.

56 J. A. Varela, M. G. Bexiga, C. Åberg, J. C. Simpson and K. A. Dawson, Quantifying size-dependent interactions between fluorescently labeled polystyrene nanoparticles and mammalian cells, *J. Nanobiotechnol.*, 2012, **10**(1), 39.

57 X. Shi, X. Wang, R. Huang, C. Tang, C. Hu and P. Ning, *et al.*, Cytotoxicity and Genotoxicity of Polystyrene Micro- and Nanoplastics with Different Size and Surface Modification in A549 Cells, *Int. J. Nanomed.*, 2022, **17**, 4509–4523.

